Mechanistic studies of the agmatine deiminase from *Listeria monocytogenes*

Charles A. Soares* and Bryan Knuckley*[1]

*Department of Chemistry, University of North Florida, Jacksonville, FL 32224, U.S.A.

Listeria monocytogenes is a Gram-positive food-borne pathogen that is capable of living within extreme environments (i.e. low temperatures and pH). This ability to survive in such conditions may arise, at least in part, from agmatine catabolism via the agmatine deiminase system (AgDS). This catabolic pathway utilizes an agmatine deiminase (AgD) to hydrolyse agmatine into *N*-carbamoylputrescine (NCP), with concomitant release of ammonia, which increases the pH, thus mitigating the ill effects of the acidic environment. Given the potential significance of this pathway for cell survival, we set out to study the catalytic mechanism of the AgD encoded by *L. monocytogenes*. In the present paper, we describe the catalytic mechanism employed by this enzyme based on pH profiles, pK_a measurements of the active site cysteine and solvent isotope effects (SIE). In addition, we report inhibition of this enzyme by two novel AgD inhibitors, i.e. *N*-(4-aminobutyl)-2-fluoro-ethanimidamide (ABFA) and *N*-(4-aminobutyl)-2-chloro-ethanimidamide (ABCA). In contrast with other orthologues, *L. monocytogenes* AgD does not use the reverse protonation or substrate-assisted mechanism, which requires an active site cysteine with a high pK_a and has been commonly seen in other members of the guanidinium-modifying enzyme (GME) superfamily. Instead, the *L. monocytogenes* AgD has a low pK_a cysteine in the active site leading to an alternative mechanism of catalysis. This is the first time that this mechanism has been observed in the GME superfamily and is significant because it explains why previously developed mechanism-based inactivators of AgDs are ineffective against this orthologue.

Key words: agmatine deiminase, guanidinium, *Listeria monocytogenes*, substrate-assisted.

INTRODUCTION

Listeriosis is an invasive infection by the Gram-positive bacterium *Listeria monocytogenes* that can lead to miscarriages in pregnant women, meningitis in newborns and death in immuno-compromised individuals [1]. This bacterial pathogen, which is most commonly found in dairy products, meats and seafood, is the third leading cause of death among food-borne pathogens [2]. Low levels of *L. monocytogenes* have also been detected in both eggs and potatoes [1]. The prevalence of food-borne illnesses associated with this organism can be attributed to its high tolerance for extreme environmental conditions, such as low temperature and pH: *L. monocytogenes* can survive at less than 4 °C and will tolerate the acidic environment found in the gastrointestinal tract [1].

L. monocytogenes possess a four-gene operon (AguABCD) that encodes a so-called agmatine deiminase system (AgDS), which is required for agmatine catabolism [3]. Analogous AgDSs are found in other bacterial species, such as *Enterococcus faecalis* and *Streptococcus mutans,* where they are believed to increase acid tolerance and confer a competitive advantage [4,5]. Agmatine is generated from arginine by arginine decarboxylase, which is found in both humans and bacteria. Agmatine enters the AgDS where is it first hydrolysed to *N*-carbamoylputrescine (NCP) with concomitant release of ammonia by agmatine deiminase (AgD). The resulting NCP is further processed by *N*-carbamoylputrescine aminohydrolase (CPA) to form putrescine and carbamoyl phosphate, which is then converted into ATP and ammonia by putrescine transcarbamoylase (PTC) (Figure 1) [6]. At low pH, transcription of the AgDS is activated leading to an increased agmatine catabolism [6]. This increase yields higher levels of ammonia and additional ATP production, which is likely to provide a competitive advantage to the bacteria in the form of acid neutralization and increased energy production. Notably, deletion of the AgD in *L. monocytogenes* attenuates pathogen survival within acidic environments, which indicates that the AgDS and, more specifically, AgD is critical for acid tolerance [6].

AgDs belongs to a larger superfamily of guanidinium-modifying enzymes (GMEs) that includes protein arginine deiminases (PADs), dimethylarginine dimethylaminohydrolases (DDAHs), amidinotransferases (ATs) and dihydrolases. Members of the GME family share a conserved catalytic Cys-His dyad that catalyses the hydrolysis of guanidinium groups of arginine, agmatine or methylarginine to ureido-containing products. To date, AgDs from a number of bacterial species, including *Helicobacter pylori*, *Porphyromonas gingivalis* and *S. mutans* have been identified and characterized [7]. Recently, sequence analysis identified a putative AgD from the genome of *L. monocytogenes* that was subsequently isolated and confirmed as a genuine AgD [6].

Previously studied bacterial AgDs from *H. pylori*, *S. mutans* and *P. gingivalis* all use a conserved active site cysteine residue for nucleophilic attack on the guanidinium group of agmatine, as well as a conserved histidine residue as a general acid/base throughout catalysis [7,8]. Using insights gained from mechanistic studies, mechanism-based inhibitors were developed to target and inactivate these AgD enzymes. The most potent inhibitors to

Abbreviations: ABCA, *N*-(4-aminobutyl)-2-chloro-ethanimidamide; ABFA, *N*-(4-aminobutyl)-2-fluoro-ethanimidamide; AgD, agmatine deiminase; AgDS, agmatine deiminase system; AT, amidinotransferase; DDAH, dimethylarginine dimethylaminohydrolase; GME, guanidinium-modifying enzyme; NCP, *N*-carbamoylputrescine; PAD, protein arginine deiminase; PTC, putrescine transcarbamoylase; SIE, solvent isotope effect.

[1] To whom correspondence should be addressed (email bryan.knuckley@unf.edu).

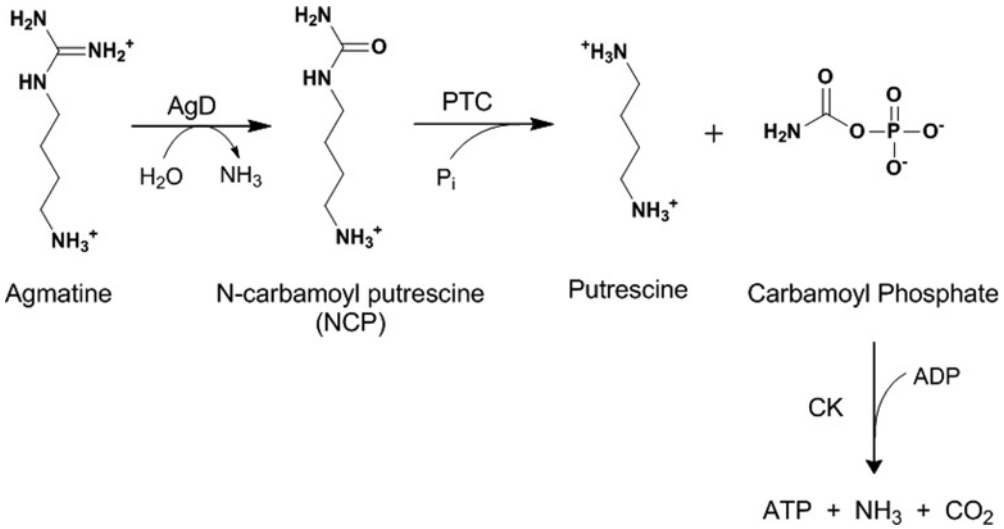

Figure 1 The AgDS found in *L. monocytogenes*

Agmatine is hydrolysed to NCP by AgD. PTC produces putrescine and carbamoyl phosphate. Finally, carbamate kinase (CK) with ADP produces ATP, ammonia and carbon dioxide from carbamoyl phosphate.

date are *N*-(4-aminobutyl)-2-fluoro-ethanimidamide (ABFA) and *N*-(4-aminobutyl)-2-chloro-ethanimidamide (ABCA), with IC_{50} values ranging from 250 nM to 15 μM for the tested AgDs [7,8].

The catalytic mechanisms for the AgD enzymes expressed by *S. mutans*, *H. pylori* and *P. gingivalis* have been identified as reverse protonation mechanisms, where the substrate preferentially binds to the deprotonated cysteine form of the enzyme [7]. This preference also means that, in a reverse protonation mechanism, the majority of the enzyme is inactive at its pH optimum (~7.5) due to the high pK_a of the cysteine residue. An alternative mechanism that has been reported for other GMEs (e.g. PAD2 and DDAH) is the substrate-assisted mechanism, wherein the proximity of the incoming positively charged substrate depresses the pK_a of the nucleophilic cysteine to promote catalysis [9,10].

Mutagenesis studies of the *L. monocytogenes* AgD demonstrated that the cysteine and histidine residues are conserved as Cys^{356} and His^{216}; however, studies to fully elucidate the catalytic mechanism have not previously been conducted. Given the therapeutic potential of this enzyme as a target against infection, we set out to elucidate the mechanism and thus gain insights to aid inhibitor development. In the present paper, we report the results of pH rate profiles, pK_a measurements of the active site cysteine residue and solvent isotope effects (SIEs). The results indicate that the AgD from *L. monocytogenes* uses a low pK_a active site cysteine in contrast with other members of this enzyme family. Given the increased reactivity of this moiety, we predict that it will be trivial to generate irreversible inhibitors targeting this unique therapeutic target.

EXPERIMENTAL

Materials

Agmatine sulfate, CHES, HEPES and MES were purchased from Sigma–Aldrich. Iodoacetamide was purchased from Chem-Impex International and 2-chloracetamidine was purchased from Oakwood Products. ABCA and ABFA were synthesized as previously reported [8]. *L. monocytogenes* AgD was synthesized based on the sequence from Cheng et al. [6] (accession number AEO05059) and cloned into a pET30a vector by GenScript.

Purification of *L. monocytogenes* AgD

The pET30a-AgD expression construct was transformed into *Escherichia coli* BL21(DE3) cells. Expression and purification of pet30a-AgD from *L. monocytogenes* was adapted from Cheng et al. [6]. Overnight cultures were grown in LB medium supplemented with 50 μg/ml kanamycin at 37 °C. Volumes of 10 ml of overnight culture were used to inoculate 1 litre of LB medium supplemented with 50 μg/ml kanamycin in a baffled flask (37 °C, 250 rev./min) until the D_{600} was 0.6–0.8. IPTG (0.4 mM) was added to the culture and the temperature was reduced to 15 °C for 12 h. The cells were harvested by centrifugation (3795 ***g*** for 10 min) and resuspended in Lysis Buffer (50 mM PBS, pH 7.4, and 10 % glycerol) before being lysed by sonication (60 % amplitude, 1 s pulse, 3 s pause, 3 min total). The lysate was centrifuged at 12000 ***g*** for 20 min and the cleared lysate was applied to the nickel column. The column was washed with PBS and PBS with 500 mM NaCl, followed by increasing concentrations of imidazole (0–500 mM). Collected fractions were analysed by SDS/PAGE (12 % gel). Fractions with >95 % purity were dialysed and stored in long term storage buffer (50 mM PBS, pH 7.4, with 20 % glycerol). A single band was observed on the SDS/PAGE gel at the expected molecular mass of 46.8 kDa (Figure 2A). Protein concentration was determined using the Bradford assay.

Kinetic assay

The production of ureido-containing compounds as a result of AgD activity was monitored using a previously established discontinuous assay that monitors the production of ureido-containing compounds [11]. This assay is designed to react with ureido-containing compounds, such as NCP, resulting in a chromophore that absorbs at 540 nm. The steady-state kinetic parameters were determined by pre-incubating 50 mM HEPES, pH 7.5, and various concentrations of agmatine (0–10 mM) for 10 min at 25 °C prior to adding 1 μM *L. monocytogenes* AgD (60 μl total volume). Reactions were allowed to proceed for 30 min at 25 °C before being quenched and 200 μl of the COLDER solution (2.25 M H_3PO_4, 4.5 M H_2SO_4,

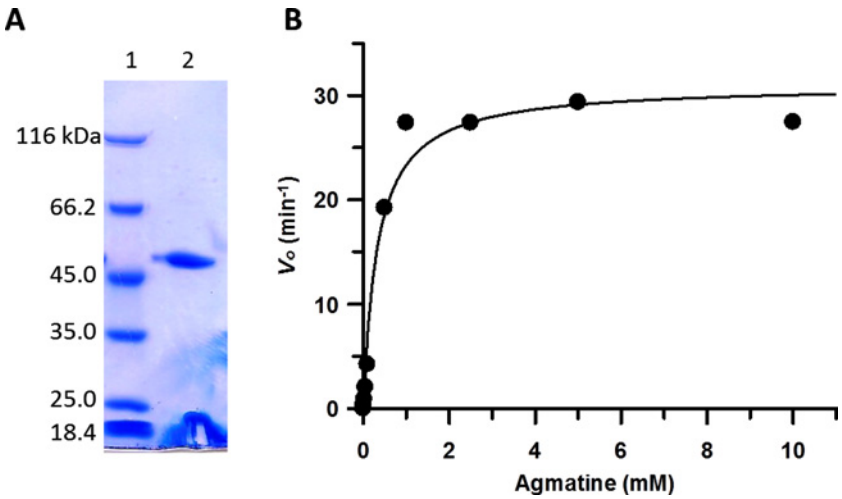

Figure 2 Purification and Michaelis–Menten kinetics of *L. monocytogenes* AgD

(**A**) SDS/PAGE analysis of purified *L. monocytogenes* AgD. Lane 1 is the molecular mass standards and lane 2 is the purified AgD. (**B**) Michaelis–Menten plot of *L. monocytogenes* AgD at the optimum pH of 7.5.

1.5 mM $NH_4Fe(SO_4)$, 20 mM diacetyl monoxime and 1.5 mM thiosemicarbizide) was subsequently added for colour development. Of note the enzymatic activity was linear with respect to time and enzyme concentration under these conditions. The mixture was vortex-mixed and incubated at 95 °C for 30 min. The absorbance was measured at 540 nm and the initial rates were fitted to eqn (1):

$$v = V_{\max}[S]/(K_m + [S]) \quad (1)$$

using GraFit version 7.0.3 software.

pH studies

pH profiles were generated for *L. monocytogenes* AgD by measuring steady-state kinetic parameters over a range of pH values (5.0–11.0) in 50 mM MES (5.0–6.5), HEPES (6.5–8.5) and CAPS (8.5–11) in the presence of various concentrations of agmatine. Reaction mixtures consisting of 50 mM buffer and agmatine (0–10 mM) were pre-incubated at 25 °C for 10 min before the addition of 1 μM *L. monocytogenes* AgD (60 μl total volume). Reactions were quenched and product formation was determined as described in the previous section. The k_{cat}/K_m and k_{cat} values obtained were plotted as a function of pH and fitted to eqn (2) (k_{cat}/K_m) or eqn (3) (k_{cat})

$$y = ((\text{Lim1} + \text{Lim2} \times 10^{(\text{pH}-\text{p}K_{a1})})/10^{(\text{pH}-\text{p}K_{a1})} + 1) - (((\text{Lim2} - \text{Lim3}) \times 10^{(\text{pH}-\text{p}K_{a2})})/(10^{(\text{pH}-\text{p}K_{a2})} + 1)) \quad (2)$$

$$y = \left((\text{Lim1} + \text{Lim2}) \times 10^{(\text{pH}-\text{p}K_a)}\right) / \left(10^{(\text{pH}-\text{p}K_a)} + 1\right) \quad (3)$$

where Lim1 is the amount of activity observed at low pH, Lim2 is pH_{opt}, Lim3 is the amount of activity observed at high pH and y represents k_{cat}/K_m.

Iodoacetamide substrate protection

A reaction mixture (480 μl total volume) consisting of 50 mM HEPES, pH 7.5, and agmatine (2 or 10 mM) was pre-incubated in the presence and absence of 3 mM iodoacetamide for 10 min at 25 °C before the addition of 1 μM *L. monocytogenes* AgD. At various time points (0, 5, 10, 15, 20, 25 and 30 min), 60 μl aliquots were removed, quenched and incubated with the COLDER solution for 30 min at 95 °C. The progress curves were fitted to eqn (4)

$$\text{NCP} = v_i(1 - e^{-k_{obs(app)}t})/k_{obs(app)} \quad (4)$$

using GraFit version 7.0.3 software.

Iodoacetamide inactivation

Inactivation of *L. monocytogenes* AgD by iodoacetamide was measured over a range of pH values (6.5–10.0) using the buffers previously listed. Time-course experiments were conducted at each pH under increasing concentrations of iodoacetamide. Briefly, 10 mM agmatine was incubated with iodoacetamide (0–20 mM) in 50 mM buffer for 10 min at 25 °C before the AgD was added to the reaction. Aliquots (60 μl) were removed at various time points (0, 5, 10, 15, 20, 25 and 30 min), quenched and incubated with 200 μl of the COLDER solution for 30 min at 95 °C. The NCP produced was quantified as previously described and plotted against time. The data were fitted to eqn (5)

$$[\text{P}] = v_i[1 - \exp^{-k_{obs(app)}t}]/k_{obs(app)} \quad (5)$$

using GraFit version 7.0.3 software, where the quantity of NCP produced is [P], the initial velocity is v_i and $k_{obs(app)}$ is the apparent pseudo-first order rate constant for the inactivation of the AgD. However, the k_{obs} values were determined by extrapolating the $k_{obs(app)}$ values to zero substrate concentration using the transformation constant described in eqn (6)

$$1 + [\text{S}]/K_m \quad (6)$$

using GraFit version 7.0.3. Following this transformation, the k_{obs} values were plotted against iodoacetamide concentration and fitted to eqn (7) to obtain the second-order rate constant, k_{inact}/K_I,

$$k_{obs} = (k_{inact}/K_I)[\text{I}] \quad (7)$$

where k_{inact} is the maximum inactivation rate and K_I is the concentration that gives half-maximum inactivation. Finally, the second-order rate constants, k_{inact}/K_I, were plotted against pH and fit to eqn (8)

$$y = \left[(Y_{min} + Y_{max}) \times 10^{pH-pK_a}\right] / \left(10^{pH-pK_a} + 1\right) \quad (8)$$

using GraFit version 7.0.3. The minimum and maximum rates of inactivation are described as Y_{min} and Y_{max} respectively.

IC_{50} determination

Reaction mixtures containing 50 mM HEPES, pH 7.5, various concentrations of the inhibitor (ABCA, ABFA or 2-chloroacetamidine), and 1 μM *L. monocytogenes* AgD were pre-incubated at 25 °C. After 15 min, 10 mM agmatine was added to the reaction mixture and incubated for an additional 30 min before being quenched. The COLDER solution (200 μl) was added, vortex-mixed and incubated at 95 °C for 30 min. The NCP produced was measured as described in the above sections and the rates were subsequently fitted to eqn (9)

$$\text{Fractional activity} = 1/(1 + [I]/IC_{50}) \quad (9)$$

using GraFit version 7.0.3 software.

Solvent isotope effects

Buffers and substrate were made in ^2H_2O for all SIE assays. The pD (p^2H) values of the buffers were determined using the formula pD = pH + 0.4 [12]. All reactions were prepared in 50 mM buffer with various concentrations of agmatine (0–10 mM) in $\geqslant$ 95 % ^2H_2O. The reactions and data analysis were performed exactly the same as described previously in the pH studies section.

RESULTS

Steady-state kinetic parameters of *L. monocytogenes* AgD at optimum pH

Initial experiments to determine the kinetic parameters for the AgD from *L. monocytogenes* were conducted at the optimal pH of 7.5 with increasing concentrations of agmatine. The deiminase activity was linear with respect to time and enzyme concentration (Supplementary Figures S1A and S1B) and the kinetic parameters were found to be $k_{cat} = 0.517 \pm 0.027$ s^{-1}, $K_m = 330 \pm 90.0$ μM and $k_{cat}/K_m = 1.57 \times 10^3$ M^{-1}·s^{-1} (Figure 2B). These values are in agreement with the previously published values of 0.572 ± 0.051 s^{-1} for k_{cat}, 650 ± 230 μM for K_m and a k_{cat}/K_m of 8.80×10^2 M^{-1}·s^{-1} [6].

pH studies

The steady-state kinetic parameters of *L. monocytogenes* AgD were determined over a pH range of 5.5–11 to aid in the elucidation of the catalytic mechanism. The pH profile curve for log k_{cat}/K_m fitted well to a model in which only one ionizable group contributes to substrate capture. The pK_a value for the ascending limb of the pH profile is 5.0 ± 1.0 (Figure 3A). The plot of k_{cat} against pH is bell-shaped and fits to a model with two apparent pK_a values and a non-limiting zero plateau for the upper limit of 0.3 ± 0.1. The ascending limb has a pK_a value of 6.2 ± 0.50 and the descending limb has a pK_a value of 9.4 ± 0.20 (Figure 3B). Deiminase activity was linear with respect to time over the pH range, indicating that the loss of activity at pH extremes is not due to an effect on enzyme stability. The pK_a values identified from the pH profiles presumably correspond to the active site residues, Cys^{356} and His^{216}. More specifically, the ascending limb of the pK_a profile probably corresponds to Cys^{356} and the descending limb to His^{216}, thus maximizing the amount of active enzyme at the optimum pH (pH of 7.5).

pK_a measurements of the active site cysteine (Cys^{356}) by iodoacetamide inactivation kinetics

To correctly identify the ionization state of Cys^{356} in the catalytic mechanism, the rates of AgD inactivation by iodoacetamide were determined as a function of pH. Iodoacetamide is a well-known non-specific affinity label for cysteine residues that has been used in elucidating the mechanisms of other GME family members (PADs, DDAH and other AgDs) [9,10,13,14]. For these experiments, the enzyme was incubated with various concentrations of iodoacetamide for a specific amount of time prior to measurement of residual activity (Figure 4A). From these plots, the pseudo-first-order rate constant of inactivation, k_{obs}, was determined and plotted as a function of iodoacetamide concentration (Figure 4B). Subsequently, the values of k_{inact}/K_I were determined from either the slope of the line or from the ratio of k_{inact} and K_I. To obtain the pK_a value of Cys^{356}, k_{inact}/K_I values were plotted as a function of pH and fitted to eqn (8) (Figure 4C). Based on the data acquired from the inactivation of the AgD with

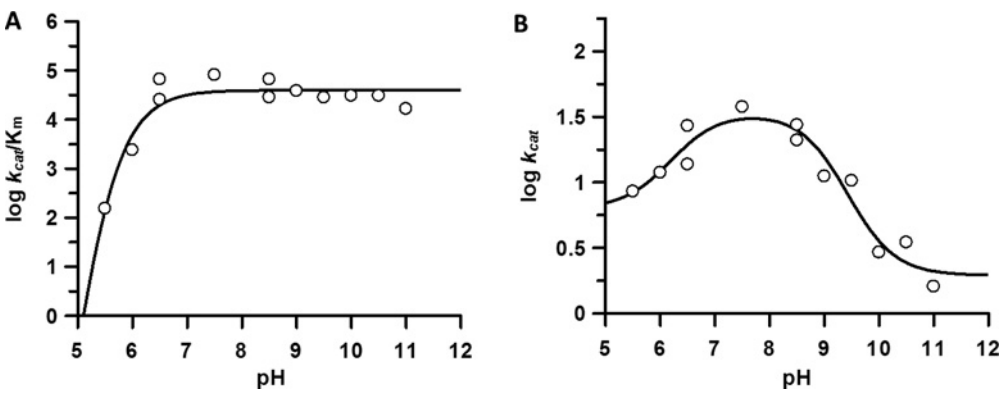

Figure 3 pH profile of *L. monocytogenes* AgD

(**A**) Plot of log k_{cat}/K_m against pH and (**B**) plot of log k_{cat} against pH for *L. monocytogenes* AgD.

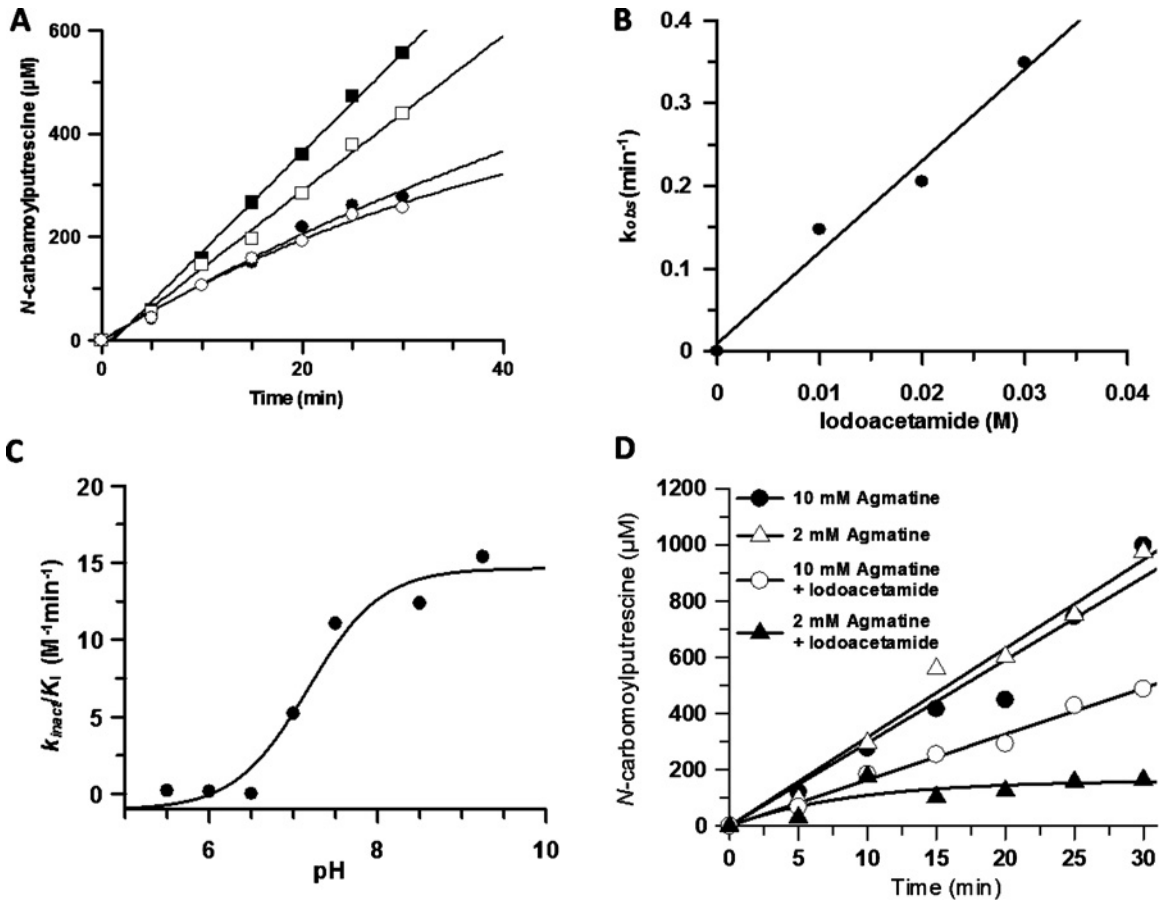

Figure 4 pK_a measurements of the active site cysteine (Cys^{356})

(**A**) Inactivation of *L. monocytogenes* AgD by various concentrations of iodoacetamide at pH 7.5: (■) 0 mM, (□) 10 mM, (●) 20 mM and (○) 30 mM iodoacetamide. (**B**) Plot of the pseudo-first-order rate constant of inactivation (k_{obs}) against iodoacetamide concentration. (**C**) Plot of k_{inact}/K_I against pH identifying the pK_a of Cys^{356}, i.e. the second-order rate constant of inactivation. (**D**) Substrate protection experiments with *L. monocytogenes* AgD demonstrates that the substrate can protect against iodoacetamide inactivation.

iodoacetamide, the pK_a of Cys^{356} was determined to be 7.2 ± 0.2, which is in reasonable agreement with the ascending limb of the log k_{cat}/K_m against pH rate profile. This value is much lower than the pK_a values obtained for the active site cysteine of other GMEs, such as the AgDs from *H. pylori*, *S. mutans* and *P. gingivalis* [7]. These enzymes deviate from the simplest assumption that the majority of the enzyme is in the active form at optimum pH (i.e. a reverse protonation mechanism). Instead, the active site cysteine residue from the *L. monocytogenes* AgD displays a much lower pK_a (pK_a of ~7 instead of ~9) and results in the majority of the enzyme in the active form. Thus, this implies that the cysteine exists mostly as the thiolate at the optimum pH. It should also be noted that substrate is able to protect against inactivation, indicating that the iodoacetamide specifically reacts with Cys^{356}, the active site cysteine (Figure 4D).

Solvent isotope effects

Since *L. monocytogenes* catalyses a reaction involving a nucleophilic thiolate, the steady-state kinetic parameters were determined in ⩾95 % ^2H_2O to provide a better understanding of the catalytic mechanism. The log k_{cat}/K_m in ^2H_2O was plotted against pD and compared with the plot of log k_{cat}/K_m in H_2O against pH (Figure 5). Of note the data from the log k_{cat}/K_m in H_2O were from Figure 3. The results with respect to k_{cat}/K_m indicate

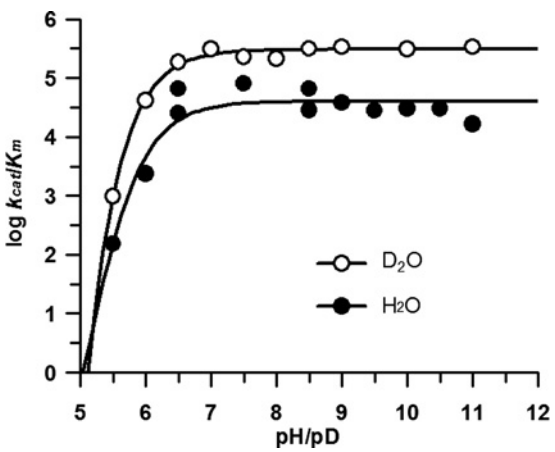

Figure 5 SIEs *for L. monocytogenes* AgD

Plot of log k_{cat}/K_m against pH/pD in (●) H_2O and (○) ^2H_2O.

that the reaction is faster in ^2H_2O and illustrate an inverse SIE of 0.4 ± 0.2 (k_{cat}/K_m^H /k_{cat}/K_m^D). By contrast, a normal SIE on k_{cat} was observed with a k_{cat}^H/k_{cat}^D of 2.1 ± 0.16.

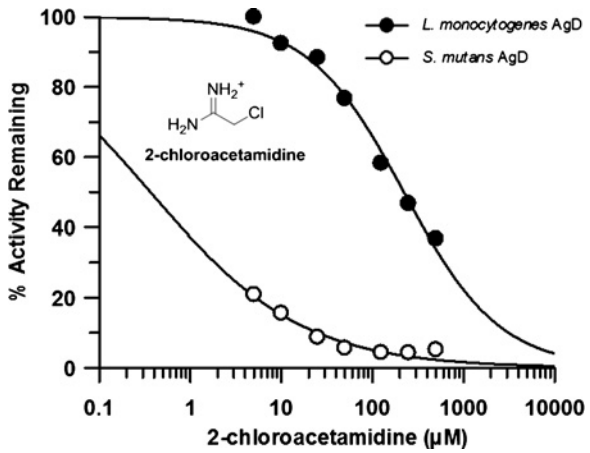

Figure 6 IC_{50} plots of *L. monocytogenes* AgD and *S. mutans* AgD for 2-chloroacetamidine

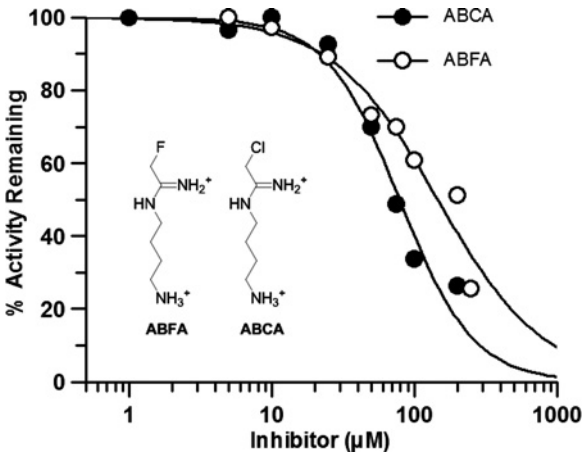

Figure 7 IC_{50} plots of *L. monocytogenes* AgD for ABFA and ABCA

An inverse SIE on k_{cat}/K_m has been observed in other GME family members containing a nucleophilic thiolate in the active site [7,13–15]. It has been suggested that the inverse SIE is a result of some GME family members utilizing a thiolate/imidazolium ion pair [7,13,14]. The fractionation factor of a thiol in ^2H_2O is approximately 0.5, and suggests that there is an increased concentration of the thiolate species. The inverse SIE observed on k_{cat}/K_m (0.41) in ^2H_2O is similar to the fractionation factor described above, and these data suggest that the increased reactivity in ^2H_2O is a result of the increased concentration of thiolate.

IC_{50} values for 2-chloroacetamidine, ABCA and ABFA

The results from the SIE and pH profiles support a mechanism utilizing a low-pK_a cysteine residue for catalysis. Since the mechanism for *L. monocytogenes* AgD differs from other bacterial AgDs, we sought to determine the potency of known cysteine inactivators and other well-studied AgD inhibitors. The inactivation of *L. monocytogenes* AgD with 2-chloroacetamidine, a positively charged inactivator that has been used in previous mechanistic reports of GME family members, was measured and the IC_{50} value was determined [7,9,13,14,16]. In previously published mechanistic studies of GME family members, such as DDAH and PAD2, 2-chloroacetamidine was used to confirm a substrate-assisted mechanism [9,10]. For these studies, a large shift in the pK_a of the active site cysteine was observed with 2-chloracetamidine in comparison with iodoacetamide due to the perturbation of the active site cysteine pK_a by the positively charged substrate [10]. The IC_{50} value of 2-chloracetamidine was determined as 221 ± 17.0 mM for *L. monocytogenes* (Figure 6). This finding was surprising given that the IC_{50} value for 2-chloroacetamidine against the AgD from *S. mutans* is 0.4 ± 0.1 mM, a >550-fold difference (Figure 6). It is also noteworthy that a similar difference was observed for iodoacetamide (Supplementary Figures S2A and S2B). Given the high concentration of 2-chloroacetamidine required for enzyme inactivation, it was not feasible to measure the pK_a of the active site cysteine using this compound.

The IC_{50} values for other well-studied AgD inactivators, ABFA and ABCA, against the *L. monocytogenes* AgD were determined. ABFA and ABCA inhibit this enzyme with IC_{50} values of 146 ± 15.0 and 78.5 ± 1.70 μM respectively (Figure 7). ABFA and ABCA are the most potent inactivators described for *H. pylori*, *S. mutans* and *P. gingivalis* to date. For example, the IC_{50} values for ABFA and ABCA against the *S. mutans* AgD are 0.27 ± 0.10 and 0.26 ± 0.61 μM respectively [7,8]. The difference in inhibition of *S. mutans* AgD and *L. monocytogenes* AgD for ABFA and ABCA are >300-fold for ABCA and >500-fold for ABFA.

DISCUSSION

The guanidinium-modifying family of enzymes is composed of the AgDs, DDAHs, PADs and ATs, which are all associated with a number of human diseases (e.g. bacterial infections, cancer, rheumatoid arthritis and colitis) [17,18]. For this reason, many of these enzymes have been identified as potential therapeutic targets and subjects of several studies to evaluate features that may be exploited for inhibitor design. One such feature is the highly conserved active site cysteine residue that acts as a nucleophile to attack the guanidinium of the substrate during catalysis. The actual mechanisms of catalysis, however, have been shown to vary between GME family members. For example, DDAH and PAD2 both utilize a substrate-assisted mechanism in which binding of the positively charged substrate to the thiol form of the active site cysteine perturbs its pK_a, thereby increasing the reactivity of the thiolate [9,10]. In contrast, PAD4 and other AgDs (*S. mutans*, *P. gingivalis* and *H. pylori*) employ a reverse protonation mechanism in which the substrate preferentially binds to the thiolate form of the free enzyme [7,13,14]. Based on previous studies, a general mechanism of catalysis has been proposed for the AgD enzymes [10,19,20]. The physiological implication of the diversity observed among members of the GME family is unclear.

Recent mutagenesis studies on the *L. monocytogenes* AgD have identified Asp^{94}, His^{216}, Asp^{218} and Cys^{356} as the four conserved catalytic residues [6]. Asp^{94} and Asp^{218} are believed to correctly orient the substrate in the active site allowing Cys^{356} to attack the substrate guanidinium. This attack leads to formation of a tetrahedral intermediate, and His^{216} can act as a general acid to donate a proton to the departing amine during collapse of the intermediate or during its formation. His^{216} can also act as a general base to abstract a proton from an active site water molecule to activate it for nucleophilic attack on the thiouronium intermediate, which ultimately leads to hydrolysis (Figure 8).

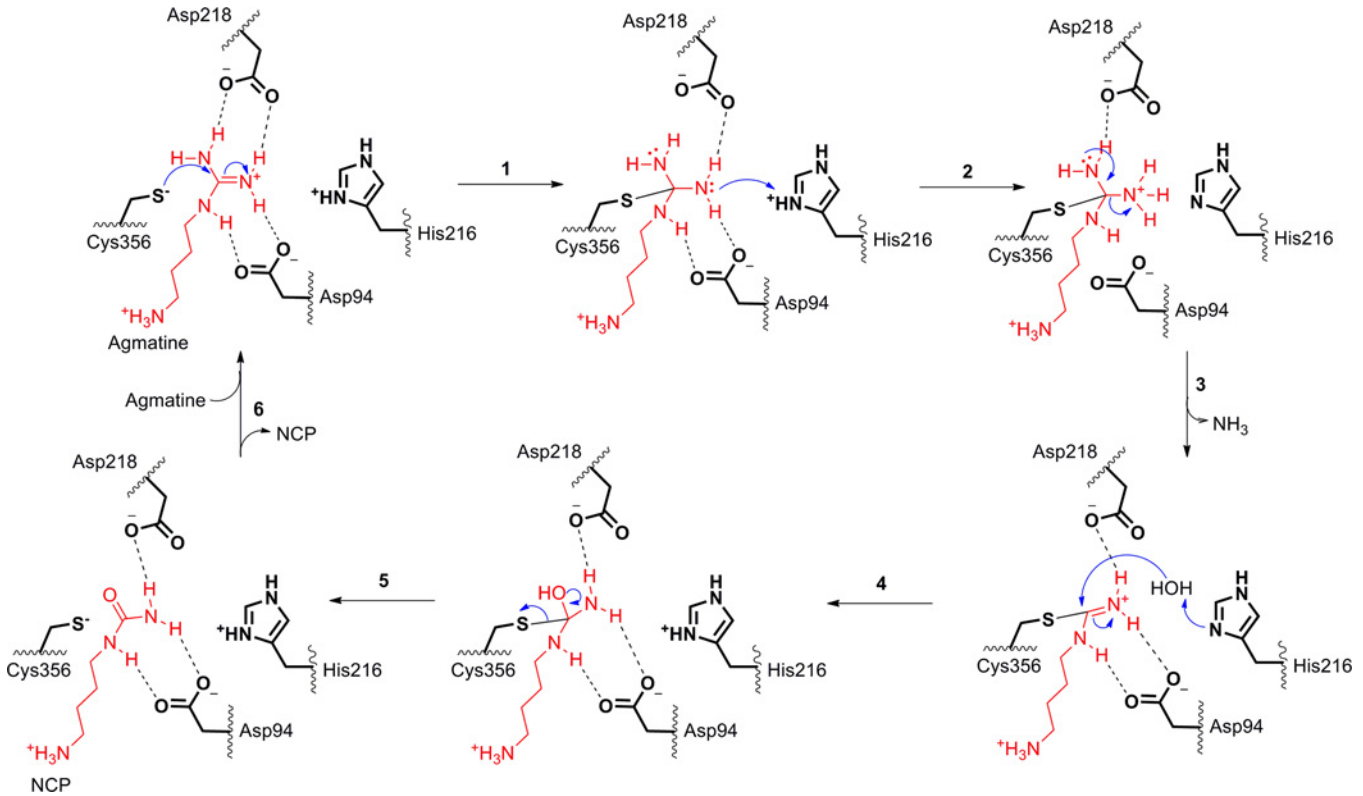

Figure 8 Proposed mechanism of catalysis for *L. monocytogenes* AgD

Given the conserved active site found in the AgD encoded by *L. monocytogenes*, we set out to determine the catalytic mechanism utilized by this enzyme. Analysis of the pH profile for k_{cat}/K_m shows a sigmoidal curve, and the decrease in activity at low pH suggests that the protonation state of only a single ionizable group is critical for substrate capture. However, the pH profiles for k_{cat} are bell-shaped, suggesting that two ionizable groups are important for the rate-limiting step of the reaction. These two ionizable groups, with pK_a values of ~6.2 and ~9.4, are most likely to be Cys^{356} and His^{216} respectively. Correctly assigning the pK_a values of Cys^{356} and His^{216} as the ascending or descending limb of the pH profile requires additional experimental data. For these assignments, the rates of inactivation by iodoacetamide were measured over a range of pH values to identify the pK_a of Cys^{356}. This rate increased with pH and resulted in a pK_a value of 7.2, which is in reasonable agreement with the ascending limb of the pH profile, suggesting it as the pK_a of Cys^{356}. Based on these observations, we can assign the ascending limb of the pH profile to Cys^{356} and the descending limb to His^{216}. Therefore, it is likely that the AgD in *L. monocytogenes* AgD utilizes a catalytic mechanism in which the active site cysteine has a low pK_a. Interestingly, the *L. monocytogenes* utilizes a catalytic mechanism more analogous to papain, a cysteine protease. In papain, the nucleophilic cysteine has a low pK_a and a higher than expected pK_a for the active site histidine [15]. Originally, it was widely believed that the PADs would utilize a mechanism similar to the cysteine proteases; however, until now this had not been observed [13].

Bacterial AgDs, PADs and even papain have displayed an inverse SIE on k_{cat}/K_m, and this inverse SIE has been attributed to an increase in the concentration of thiolate [7,13,14]. In ^2H_2O, the concentration of the reactive thiolate can be increased approximately 2-fold; the fractionation factor of a thiol in ^2H_2O is ~0.5. For *L. monocytogenes*, we observed an inverse SIE on k_{cat}/K_m of 0.4 ± 0.2, which correlates with the fractionation factor of the thiol in ^2H_2O. Based on these data, the higher rate observed in ^2H_2O is most likely to be due to an equilibrium proton transfer to solvent leading to a higher concentration of reactive thiolate. A normal SIE is observed for GME family members that utilize a substrate-assisted mechanism because the higher concentration of thiolate in ^2H_2O has no effect on k_{cat}/K_m since the enzyme binds the substrate as either the thiol or thiolate. Of note, a normal isotope effect on k_{cat} is expected and suggests that proton transfer contributes significantly to the rate-limiting step of the reaction.

Based on these data, Cys^{356} exist as a thiolate and His^{216} is protonated in the active form of the *L. monocytogenes* AgD. Thus, at low pH (pH <5), the active site cysteine exists as the thiol and the histidine contains a positively charged imidazolium side chain. As pH increases, the concentration of thiolate increases and substrate binding increases, as evident by the ascending limb of the pH profile. At a pH above the optimum, a high concentration of the thiolate exists, which increases affinity for the substrate. In addition, the concentration of the deprotonated His^{216} increases, leading to a reduction in positive charge of the active site and promotes binding of the agmatine, which is evident by the lack of a descending limb of the log k_{cat}/K_m pH profile. The lack of a descending limb in the pH profile of log k_{cat}/K_m may suggests proton transfer from His^{216} occurs after or concomitantly with collapse of the tetrahedral intermediate.

Recently, two novel haloacetamidine-based AgD inactivators (ABCA and ABFA) have been developed and are the most potent AgD inhibitors described to date [7,8,21,22]. Since

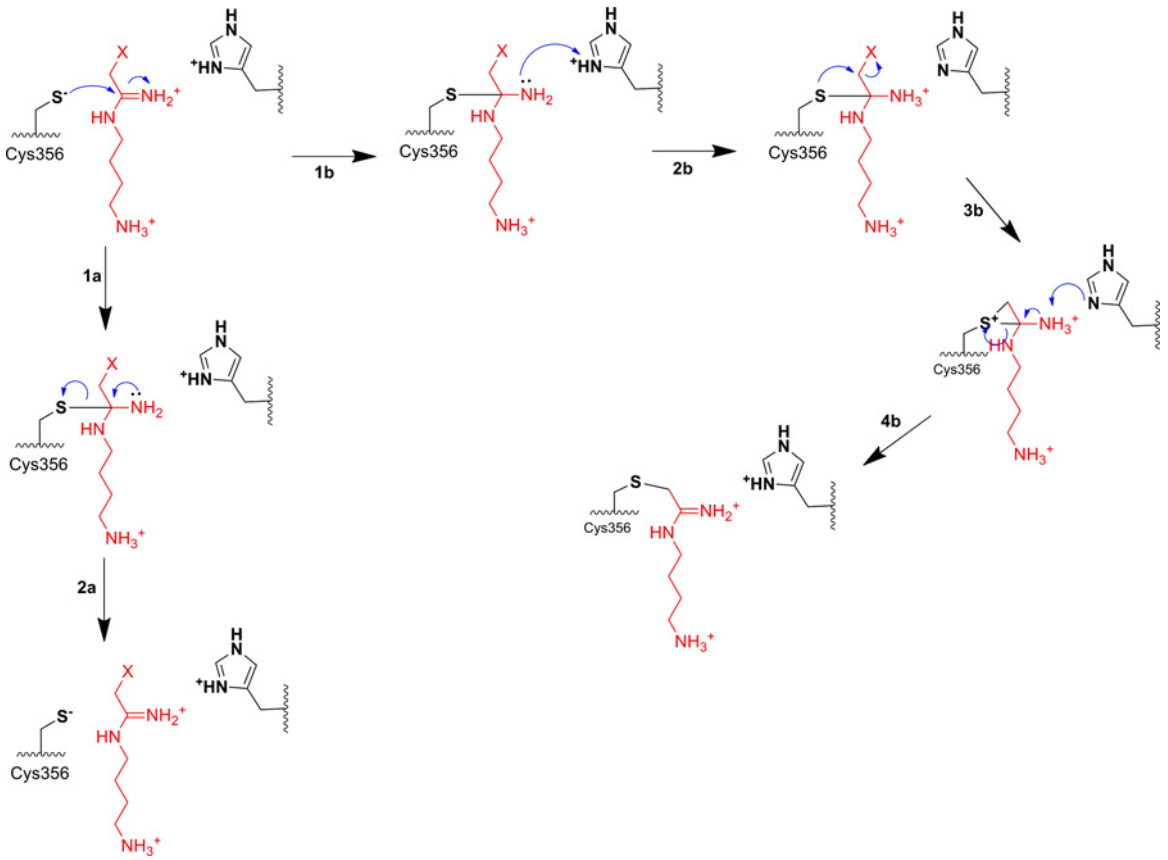

Figure 9 Influence of the active site histidine pK_a on AgD inactivation by ABFA or ABCA

Proposed mechanism of AgD inactivation by a high-pK_a histidine as seen in *L. monocytogenes* (steps 1a–2a) or by a low-pK_a histidine as seen in *H. pylori*, *S. mutans* or *P. gingivalis* (steps 1b–4b).

L. monocytogenes AgD utilizes a conserved active site cysteine, we evaluated the effectiveness of these mechanism-based inactivators on this enzyme. Interestingly, the IC_{50} values for ABCA and ABFA against *L. monocytogenes* AgD are much higher than those for other AgDs. The loss in potency for these inhibitors may be due to the high pK_a of His^{216} (pK_a $\sim$ 9.5). Previously characterized AgDs (*S. mutans*, *H. pylori* and *P. gingivalis*) and PADs (e.g. PAD1, PAD3 and PAD4) utilize a reverse protonation mechanism, where the active site histidine has a much lower pK_a (pK_a $\sim$ 6). Furthermore, previous studies of the PAD inhibitors, F- and Cl-amidine, suggests that protonation of the inhibitor by the active site histidine prior to collapse of the tetrahedral intermediate is a critical step for complete inactivation [23]. For example, in previously studied AgDs, the inhibitors ABCA and ABFA would bind to the enzyme, undergo nucleophilic attack by the active site cysteine and be stabilized through protonation of the intermediate by the active site histidine. This step leads to halide displacement forming the three-membered sulfonium ring, and ultimately results in the inactivated enzyme (Figure 9, steps 1b–4b). However, the results from the present study suggest an alternative mechanism of inactivation. The AgD from *L. monocytogenes* incorporates an active site histidine with a much higher pK_a than other AgDs or related GME family members, which means that after nucleophilic attack, proton transfer to the intermediate is too slow and the intermediate collapses before halide displacement, which results in the regeneration of free enzyme (Figure 9, steps 1a–2a). Further work will be needed to clarify these differences for developing more potent inhibitors to this bacterial AgD. In addition, the increased reactivity of the active site cysteine in this orthologue could be exploited through the use of different warheads.

AUTHOR CONTRIBUTION

Charles Soares conducted most of the experiments, analysed results and wrote some of the paper. Bryan Knuckley conceived the idea, conducted experiments, analysed results and wrote the paper with Charles Soares.

ACKNOWLEDGEMENTS

We thank Dr Corey Causey and Dr Paul R. Thompson for helpful and insightful discussions.

FUNDING

This work was supported by the UNF startup funds; and the UNF Faculty Development Research Grant.

REFERENCES

1 Farber, J.M. and Peterkin, P.I. (1991) *Listeria monocytogenes*, a food-borne pathogen. Microbiol. Rev. **55**, 476–511 PubMed

2 Ramaswamy, V., Cresence, V.M., Rejitha, J.S., Lekshmi, M.U., Dharsana, K.S., Prasad, S.P. and Vijila, H. M. (2007) Listeria – review of epidemiology and pathogenesis. J. Microbiol. Immunol. Infect. **40**, 4–13 PubMed

3 Chen, J., Cheng, C., Xia, Y., Zhao, H., Fang, C., Shan, Y., Wu, B. and Fang, W. (2011) Lmo0036, an ornithine and putrescine carbamoyltransferase in *Listeria monocytogenes*, participates in arginine deiminase and agmatine deiminase pathways and mediates acid tolerance. Microbiology **157**, 3150–3161 CrossRef PubMed

4 Griswold, A.R., Jameson-Lee, M. and Burne, R.A. (2006) Regulation and physiologic significance of the agmatine deiminase system of *Streptococcus mutans* UA159. J. Bacteriol. **188**, 834–841 CrossRef PubMed

5 Llácer, J.L., Polo, L.M., Tavárez, S., Alarcón, B., Hilario, R. and Rubio, V. (2007) The gene cluster for agmatine catabolism of *Enterococcus faecalis*: study of recombinant putrescine transcarbamylase and agmatine deiminase and a snapshot of agmatine deiminase catalyzing its reaction. J. Bacteriol. **189**, 1254–1265 CrossRef PubMed

6 Cheng, C., Chen, J., Fang, C., Xia, Y., Shan, Y., Liu, Y., Wen, G., Song, H. and Fang, W. (2013) Listeria monocytogenes aguA1, but not aguA2, encodes a functional agmatine deiminase: biochemical characterization of its catalytic properties and roles in acid tolerance. J. Biol. Chem. **288**, 26606–26615 CrossRef PubMed

7 Jones, J.E., Dreyton, C.J., Flick, H., Causey, C.P. and Thompson, P.R. (2010) Mechanistic studies of agmatine deiminase from multiple bacterial species. Biochemistry **49**, 9413–9423 CrossRef PubMed

8 Jones, J.E., Causey, C.P., Lovelace, L., Knuckley, B., Flick, H., Lebioda, L. and Thompson, P.R. (2010) Characterization and inactivation of an agmatine deiminase from *Helicobacter pylori*. Bioorg. Chem. **38**, 62–73 CrossRef PubMed

9 Dreyton, C.J., Knuckley, B., Jones, J.E., Lewallen, D.M. and Thompson, P.R. (2014) Mechanistic studies of protein arginine deiminase 2: evidence for a substrate-assisted mechanism. Biochemistry **53**, 4426–4433 CrossRef PubMed

10 Stone, E.M., Costello, A.L., Tierney, D.L. and Fast, W. (2006) Substrate-assisted cysteine deprotonation in the mechanism of dimethylargininase (DDAH) from *Pseudomonas aeruginosa*. Biochemistry **45**, 5618–5630 CrossRef PubMed

11 Knipp, M. and Vasák, M. (2000) A colorimetric 96-well microtiter plate assay for the determination of enzymatically formed citrulline. Anal. Biochem. **286**, 257–264 CrossRef PubMed

12 Glasoe, P.K. and Long, F.A. (1960) Use of glass electrodes to measure acidities in deuterium oxide. J. Phys. Chem. **64**, 188–190 CrossRef

13 Knuckley, B., Bhatia, M. and Thompson, P.R. (2007) Protein arginine deiminase 4: evidence for a reverse protonation mechanism. Biochemistry **46**, 6578–6587 CrossRef PubMed

14 Knuckley, B., Causey, C.P., Jones, J.E., Bhatia, M., Dreyton, C.J., Osborne, T.C., Takahara, H. and Thompson, P.R. (2010) Substrate specificity and kinetic studies of PADs 1, 3, and 4 identify potent and selective inhibitors of protein arginine deiminase 3. Biochemistry **49**, 4852–4863 CrossRef PubMed

15 Lewis, S.D., Johnson, F.A. and Shafer, J.A. (1981) Effect of cysteine-25 on the ionization of histidine-159 in papain as determined by proton nuclear magnetic resonance spectroscopy. Evidence for a his-159–Cys-25 ion pair and its possible role in catalysis. Biochemistry **20**, 48–51 CrossRef PubMed

16 Stone, E.M., Schaller, T.H., Bianchi, H., Person, M.D. and Fast, W. (2005) Inactivation of two diverse enzymes in the amidinotransferase superfamily by 2-chloroacetamidine: dimethylargininase and peptidylarginine deiminase. Biochemistry **44**, 13744–13752 CrossRef PubMed

17 Jones, J.E., Causey, C.P., Knuckley, B., Slack-Noyes, J.L. and Thompson, P.R. (2009) Protein arginine deiminase 4 (PAD4): current understanding and future therapeutic potential. Curr. Opin. Drug Discov. Devel. **12**, 616–627 PubMed

18 Wang, Y., Hu, S., Gabisi, A. M., Er, J.A., Pope, A., Burstein, G., Schardon, C.L., Cardounel, A.J., Ekmekcioglu, S. and Fast, W. (2014) Developing an irreversible inhibitor of human DDAH-1, an enzyme upregulated in melanoma. ChemMedChem **9**, 792–797 CrossRef PubMed

19 Li, Z., Kulakova, L., Li, L., Galkin, A., Zhao, Z., Nash, T.E., Mariano, P.S., Herzberg, O. and Dunaway-Mariano, D. (2009) Mechanisms of catalysis and inhibition operative in the arginine deiminase from the human pathogen *Giardia lamblia*. Bioorg. Chem. **37**, 149–161 CrossRef PubMed

20 Galkin, A., Lu, X., Dunaway-Mariano, D. and Herzberg, O. (2005) Crystal structures representing the Michaelis complex and the thiouronium reaction intermediate of Pseudomonas aeruginosa arginine deiminase. J. Biol. Chem. **280**, 34080–34087 CrossRef PubMed

21 Thomson, A., O'Connor, S., Knuckley, B. and Causey, C.P. (2014) Design, synthesis, and *in vitro* evaluation of an activity-based protein profiling (ABPP) probe targeting agmatine deiminases. Bioorg. Med. Chem. **22**, 4602–4608 CrossRef PubMed

22 Marchenko, M., Thomson, A., Ellis, T.N., Knuckley, B. and Causey, C.P. (2015) Development of a clickable activity-based protein profiling (ABPP) probe for agmatine deiminases. Bioorg. Med. Chem. **23**, 2159–2167 CrossRef PubMed

23 Knuckley, B., Causey, C.P., Pellechia, P.J., Cook, P.F. and Thompson, P.R. (2010) Haloacetamidine-based inactivators of protein arginine deiminase 4 (PAD4): evidence that general acid catalysis promotes efficient inactivation. ChemBioChem **11**, 161–165 CrossRef PubMed

Received 14 March 2016/24 March 2016; accepted 30 March 2016
Accepted Manuscript online 31 March 2016, doi:10.1042/BCJ20160221